



# A dual adaptive explicit time integration algorithm for efficiently solving the cardiac monodomain equation

Konstantinos A. Mountris<sup>1,2</sup>  | Esther Pueyo<sup>1,2</sup> 

<sup>1</sup>Aragón Institute of Engineering Research, IIS Aragón, , University of Zaragoza, Zaragoza, Spain

<sup>2</sup>CIBER in Bioengineering, Biomaterials & Nanomedicine (CIBER-BBN), Madrid, Spain

## Correspondence

Konstantinos A. Mountris, Aragón Institute of Engineering Research, IIS Aragón, University of Zaragoza, Zaragoza 50018, Spain.  
Email: kmountris@unizar.es

## Funding information

European Social Fund; Gobierno de Aragón, Grant/Award Numbers: LMP124-18, T39\_20R; H2020 European Research Council, Grant/Award Number: ERC-StG-638284; Ministerio de Ciencia e Innovación, Grant/Award Number: PID2019-105674RB-I00

## Abstract

The monodomain model is widely used in *in-silico* cardiology to describe excitation propagation in the myocardium. Frequently, operator splitting is used to decouple the stiff reaction term and the diffusion term in the monodomain model so that they can be solved separately. Commonly, the diffusion term is solved implicitly with a large time step while the reaction term is solved by using an explicit method with adaptive time stepping. In this work, we propose a fully explicit method for the solution of the decoupled monodomain model. In contrast to semi-implicit methods, fully explicit methods present lower memory footprint and higher scalability. However, such methods are only conditionally stable. We overcome the conditional stability limitation by proposing a dual adaptive explicit method in which adaptive time integration is applied for the solution of both the reaction and diffusion terms. We perform a set of numerical examples where cardiac propagation is simulated under physiological and pathophysiological conditions. Results show that the proposed method presents preserved accuracy and improved computational efficiency as compared to standard operator splitting-based methods.

## KEYWORDS

adaptive explicit integration, cardiac electrophysiology, operator splitting

## 1 | INTRODUCTION

Computational modeling and simulation is widely used in cardiac electrophysiology to gain more insight into the mechanisms underlying the heart's electrical activity, predict unfavorable responses in the presence of disease or identify novel therapeutic targets. Propagation of action potential (AP) waves in the myocardium can be simulated by solving a system of partial differential equations (PDEs) known as the bidomain model.<sup>1</sup> The bidomain model considers the cardiac tissue as a continuum of two anisotropic compartments describing the intracellular and extracellular spaces. Assuming equal anisotropy ratios for the intracellular and extracellular spaces, the bidomain model can be reduced to the simplified monodomain model.<sup>2</sup> In situations where the currents in the extracellular domain have little influence on cardiac transmembrane potential and ionic currents, the monodomain model can produce realistic activation patterns and transmembrane potential values with less computational cost than the bidomain model.<sup>3</sup>

The monodomain model is described by a single reaction–diffusion PDE for the transmembrane potential across the myocardium, while the extracellular potential can be computed from another PDE once the transmembrane potential has been solved. In the reaction–diffusion PDE, the reaction term describes the generation of the cellular AP and the diffusion term describes its propagation in the tissue. Realistic cardiac cell models are composed of a large set of stiff

ordinary differential equations (ODEs) to describe the temporal evolution of the ionic concentrations and gating variables of the cell. Solving stiff ODE models can be time consuming, especially for large scale problems, since a small time integration step is required to ensure numerical stability. The operator splitting technique<sup>4</sup> can be used to decouple the stiff reaction term and the diffusion term. In this way, a larger time step can be used to solve the diffusion term independently of the reaction term, which may be solved adaptively using a small time step.<sup>5,6</sup>

Commonly, the decoupled reaction–diffusion system is solved by employing a semi-implicit scheme. The stiff reaction term is integrated using an explicit time integration method (e.g., forward Euler, Rush–Larsen<sup>7</sup>) whereas the diffusion term is solved using an implicit time integration method (e.g., backward Euler, Crank–Nicolson). Implicit time integration methods are popular for their unconditional stability. However, they require solving a system of equations at each time step, which makes them more complex to implement and harder to parallelize than explicit methods. Explicit methods, on the other hand, are only conditionally stable. Yet attractive, explicit methods are impractical for large scale problems where a high mesh resolution is required. This is so because a very small time step is required to ensure stability, as with decreasing mesh spacing the upper bound of the time step is decreased too.<sup>8</sup>

In this work, we identify a simple, yet meaningful, realization that allows overcoming the conditional stability limitation of the explicit time integration scheme. Once the reaction and diffusion terms of the monodomain model are decoupled by application of the operator splitting technique, we propose a dual adaptive explicit time integration (DAETI) method where both the reaction and diffusion terms are solved explicitly with a different adaptive scheme in each case. Since most of the computational burden is associated with the solution of the reaction term, the overhead of the adaptive solution of the diffusion term is minimum. The structure of the article is as follows. In Section 2, we describe the DAETI algorithm. In Section 3, we compare the accuracy and efficiency of the proposed method against the standard method with adaptive time integration for the reaction term only and against the method without any time step adaptation. The comparison is performed for two-dimensional (2D) and three-dimensional (3D) problems of cardiac electrophysiology in both health and disease. In Section 4, we discuss our findings and in Section 5, we present the concluding remarks.

## 2 | DUAL ADAPTIVE EXPLICIT TIME INTEGRATION

Propagation of the cardiac AP was simulated by using the monodomain model given by:

$$\begin{aligned} \partial V / \partial t &= -I_{ion}(V) / C + \nabla \cdot (\mathbf{D} \nabla V) & \text{in } \Omega \\ \mathbf{n} \cdot (\mathbf{D} \nabla V) &= 0 & \text{in } \partial \Omega \end{aligned} \quad (1)$$

where  $\partial V / \partial t$  is the time derivative of the transmembrane potential,  $I_{ion}$  is the total ionic current,  $C$  denotes the cell capacitance per unit surface area and  $\mathbf{D}$  is the diffusion tensor.  $\Omega$  and  $\partial \Omega$  denote the domain of interest and its boundary, respectively, and  $\mathbf{n}$  is the outward unit vector normal to  $\partial \Omega$ .

Employing the operator splitting method,<sup>4</sup> Equation (1) can be written as:

$$\partial V / \partial t = -I_{ion}(V) / C \text{ in } \Omega \quad (2a)$$

$$\partial V / \partial t = \nabla \cdot (\mathbf{D} \nabla V) \text{ in } \Omega \quad (2b)$$

$$\mathbf{n} \cdot (\mathbf{D} \nabla V) = 0 \text{ in } \partial \Omega \quad (2c)$$

Following Strang's operator splitting, time integration of the set of Equation (2) for the time interval  $[0, T]$  using a time step  $dt$  is performed in three steps (I–III). Taking the solution at a given time  $t$  as the initial condition, adaptive integration is applied in step I to solve the diffusion term [Equations (2b) and (2c)] with time step  $dt/2$ . Using the results of step I as initial condition, adaptive integration for the reaction term (ODEs for ionic concentrations and gating variables used in the computation of  $I_{ion}(V)$  together with Equation (2a)) is applied at step II for time step  $dt$ . Using the results of II, the iteration terminates by integrating again the diffusion term for time step  $dt/2$  in step III. In practice, steps I and III can be combined into only one step (denoted as step B), except for the initial and final steps of the integration in the interval  $[0, T]$ . Step II is denoted as step A.

In our proposed dual adaptive explicit time integration (DAETI) method, similarly to the standard adaptive time integration method,<sup>4</sup> the reaction term integration in step II was performed by using the Rush–Larsen and forward Euler methods with adaptive time step  $dt_{ar} = dt/k$ , where the parameter  $k$  was defined to be an integer so as to keep steps A and B, corresponding to the reaction and diffusion terms, synchronized every time step  $dt$ . The value of  $k$  was selected in the range  $[1, k_{max}]$ . The upperbound  $k_{max}$  was obtained as  $k_{max} = \lfloor dt/dt_0 \rfloor$ , where  $dt_0$  is the maximum value of the time step that guarantees numerical stability of the cell electrophysiology model. In each iteration, the value of the parameter  $k$  was calculated by  $k = k_0 + \lfloor |\partial V/\partial t| \rfloor$ , where  $\partial V/\partial t$  is the time derivative of the AP at the previous iteration. For  $\partial V/\partial t > 0$  (e.g., steep gradient during upstroke), we chose  $k_0 = 5$  to ensure safe propagation of the wave front. For  $\partial V/\partial t \leq 0$  (e.g., smooth gradient during repolarization), we chose  $k_0 = 1$  to avoid zero-division during the calculation of  $dt_{ar}$ . If  $k > k_{max}$ , then  $k = k_{max}$ . For a more detailed explanation on the choice of  $k_0$ , we refer the reader to Reference 4.

The adaptive time integration of the diffusion term in steps I and III was performed using the forward Euler method with time step  $dt_{ad} = dt/2l$ , where  $l = \lfloor dt/2dt_s \rfloor$  if  $dt/2 > dt_s$  and  $l = 1$ , otherwise. A stable diffusion time step  $dt_s$  was obtained by the Gerschgorin theorem<sup>9</sup>:

$$dt_s = 0.9 \min_{i=1, \dots, n} \left[ \frac{m_{ii}}{k_{ii} + \sum_{\substack{j=1 \\ j \neq i}}^n |k_{ij}|} \right]. \quad (3)$$

where  $m_{ij}$ ,  $k_{ij}$  are the elements of the  $i$ -th row and  $j$ -th column of the mass and stiffness matrices, respectively, for the Finite Element approximation of Equation (2b). The multiplication factor 0.9 is a safety factor to ensure numerical stability for the estimated time step. When  $dt/2 > dt_s$ , the adaptive integration of the diffusion term ensures numerical stability, while when  $dt/2 \leq dt_s$ , the DAETI method is reduced to the standard operator splitting-based integration.

### 3 | EVALUATION OF DUAL ADAPTIVE EXPLICIT TIME INTEGRATION

To evaluate the accuracy and efficiency of the DAETI method we performed simulations under health and disease conditions considering 2D atrial and ventricular tissue sheets, a 3D ventricular cuboid and a realistic biventricular geometry. We compared the simulation results obtained by DAETI with simulation results obtained by the operator splitting technique with no adaptive integration (OST) and by OST with adaptive integration of the reaction term (OSTAR). Both the reaction and diffusion terms in OST and OSTAR were solved explicitly using the forward Euler method as in DAETI.

The time step used in simulations with the OST method was  $dt = 0.005$  ms for atrial and  $dt = 0.01$  ms for ventricular electrophysiology. The use of the Rush–Larsen method for the integration of ionic gating variables allowed to obtain stable solutions with the selected time steps. We validated the obtained solutions against the solutions of the cell model implementations of the CellML repository using MATLAB's adaptive ODE15s method.<sup>10</sup> The respective time integration steps used in DAETI were  $dt = 0.05$  ms and  $dt = 0.1$  ms (i.e.,  $10\times$  larger than OST) for atrial and ventricular simulations. In OSTAR,  $dt = 0.05$  ms and  $dt = 0.1$  ms were used for coarse mesh discretizations where  $dt_s \geq dt$ . For fine mesh discretizations where  $dt_s < dt$ ,  $dt_s$  was used as the time integration step.

Simulations were performed using a multithreaded implementation of the Finite Element Method using ELECTRA, an in-house software implementing the Finite Element Method and the Meshfree Mixed Collocation method<sup>11–13</sup> for solving the monodomain model. In this work, we used the Finite Element implementation. All simulations were performed on a laptop with Intel® Core™ i7-4720HQ CPU and 16 GB of RAM.

#### 3.1 | Electrical propagation in 2D cardiac tissues

AP propagation in  $5 \times 5$  cm tissue sheets was simulated for  $T = 500$  ms after achieving steady-state conditions at a pacing cycle length of 1000 ms. A stimulus of 1 ms duration and twice diastolic threshold amplitude was delivered at the

left side of the tissue ( $X = 0$  cm) at time  $t = 50$  ms. 4-node regular isoparametric elements with a spacing step of  $h = 100\mu\text{m}$  were used. Homogeneous atrial and ventricular tissues were considered. In the case of the atrial tissue, cellular electrophysiology was represented by the Maleckar et al. human AP model.<sup>14</sup> In the case of the ventricular tissue, cellular electrophysiology was represented by the O'Hara et al. human epicardial AP model.<sup>15</sup> Fiber orientation was considered parallel to the X-axis for both atrial and ventricular simulations. The tissue diffusion coefficient in the longitudinal direction was  $d_0 = 0.0035$  cm<sup>2</sup>/ms for atrial and  $d_0 = 0.0017$  cm<sup>2</sup>/ms for ventricular tissue, with the transverse-to-longitudinal ratio being  $\rho = 0.2$ . The critical value for the diffusion time step  $dt_s$  was estimated using Equation (3), rendering a value of  $dt_s = 0.006$  ms for the atrial tissue simulation and  $dt_s = 0.013$  ms for the ventricular tissue simulation. For comparison, the time step limit for satisfying the Courant–Friedrichs–Lewy condition was  $dt_{CFL} = 0.19$ ms for atrial tissue and  $dt_{CFL} = 0.17$ ms for ventricular tissue.

The APs at the center of the tissue sheet calculated using the three evaluated methods are shown in Figure 1 for both atrial and ventricular tissue simulations. As can be observed from the figure, the absolute differences in transmembrane potential between DAETI and any of the other two methods were minimal for both simulations, being within 0.18 mV for the atrial tissue and 0.09 mV for the ventricular tissue. For the atrial tissue simulation, the longitudinal conduction velocity (CV) obtained using the DAETI method was  $CV = 0.056$  cm/ms, while CV values for OSTAR and OST methods were  $CV = 0.055$  cm/ms and  $CV = 0.053$  cm/ms, respectively. AP duration at 90% repolarization ( $APD_{90}$ ) was  $APD_{90} = 208.0$  ms for DAETI,  $APD_{90} = 207.6$  ms for OSTAR, and  $APD_{90} = 209.0$  ms for OST. For the ventricular tissue simulation, we obtained  $CV = 0.060$  cm/ms and  $APD_{90} = 227$  ms for the three time integration methods. Total execution time was 21 min for DAETI, 95 min for OSTAR and 103 min for OST.

### 3.2 | Electrical propagation in a 2D cardiac tissue with fibrosis

We next simulated AP propagation in a  $5 \times 5$  cm ventricular epicardial tissue sheet, as in subsection 3.1, but in this case we included 10% diffusive fibrosis by randomly distributing fibroblasts across the tissue following a uniform distribution as in Reference 16. Human ventricular epicardial cell electrophysiology was represented by the O'Hara et al. model, while fibroblast electrophysiology was represented by the MacCannell active fibroblast model.<sup>17</sup> The tissue was stimulated by applying a cross-field stimulation (S1–S2) protocol to generate a sustained spiral wave. The first stimulus (S1) was applied at the left side of the tissue ( $X = 0$  cm) at time  $t = 50$  ms, when the tissue coupling epicardial cells and fibroblasts was stabilized at a pacing cycle length of 1000 ms. A second stimulus S2 was applied at the bottom left corner of the tissue ( $X = 0 - 1.25$  cm,  $Y = 0 - 2.50$  cm) at time  $t = 200$  ms. The time for application of the S2 stimulus was chosen so that the S2 wave front interacted with the S1 wave tail and could lead to the generation of a spiral wave.

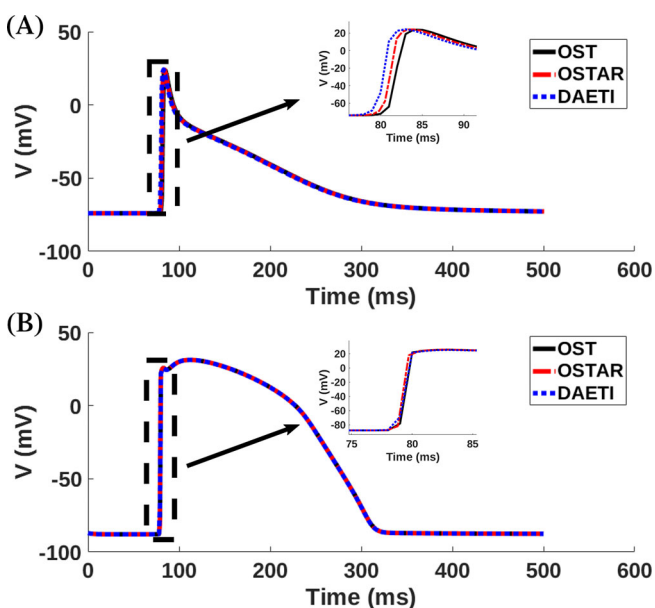


FIGURE 1 APs at the center of a  $5 \times 5$  cm human tissue sheet. (A) AP for atrial tissue simulation and (B) AP for ventricular tissue simulation using OST, OSTAR, and DAETI methods

We performed simulations on six meshes with 4-node regular elements and varying spacing steps ranging from  $h = 100$  to  $h = 200 \mu\text{m}$ . The computational efficiency of DAETI was compared against that of OSTAR and OST. The critical diffusion time step  $dt_s$  was obtained by Equation (3) for each mesh. The diffusion coefficient was  $d_{om} = 0.002 \text{ cm}^2/\text{ms}$  between epicardial myocytes and  $d_{of} = 0.00066 \text{ cm}^2/\text{ms}$  between fibroblasts as well as for the interaction between myocytes and fibroblasts. The transverse-to-longitudinal conductivity ratio was set to  $\rho = 0.25$ . The characteristics of the simulated meshes and the corresponding values of  $dt_s$  are provided in Table 1, as well as the  $dt_{CFL}$ , and the mean absolute difference between DAETI–OST ( $|DAETI - OST|$ ) and OSTAR–OST ( $|OSTAR - OST|$ ).

Transmembrane voltage in the simulated tissues after application of the cross-field stimulation protocol is presented in Figure 2 for the mesh with  $h = 100 \mu\text{m}$ . The three methods rendered highly similar voltage values, being the absolute difference between aligned APs below  $0.41 \text{ mV}$ , with the three of them presenting the same characteristics of the generated spiral waves at the different time instants along the simulation time.

The total execution time for a simulation time of  $T = 500 \text{ ms}$  is given in Figure 3A for the three evaluated methods. As can be observed from Figure 3A, the computational time required by DAETI was notably lower than that of OST. When compared to OSTAR, DAETI was associated with similar computational times for coarse meshes but with remarkably lower times for fine meshes. Furthermore, Figure 3B presents the temporal evolution of the adaptive time

**TABLE 1** Summary of mesh characteristics used in the simulation of a 2D fibrotic tissue under cross-field stimulation

$h \text{ (}\mu\text{m)}$	Nodes	Elem.	$dt_s \text{ (ms)}$	$dt_{CFL} \text{ (ms)}$	$ DAETI - OST  \text{ (mV)}$	$ OSTAR - OST  \text{ (mV)}$
200	63001	62500	0.113	0.377	0.193	0.156
180	77284	76729	0.091	0.330	0.165	0.124
160	97969	97344	0.072	0.284	0.143	0.115
140	128164	127449	0.059	0.248	0.131	0.112
120	173889	173056	0.044	0.207	0.105	0.084
100	251001	250000	0.028	0.173	0.092	0.071

Note:  $h$  denotes the mesh spacing,  $dt_s$  is the critical value for the diffusion time integration step,  $dt_{CFL}$  is the upper limit for satisfying the CFL condition,  $|DAETI - OST|$  is the mean absolute difference between DAETI and OST solutions, and  $|OSTAR - OST|$  is the mean absolute difference between OSTAR and OST solutions.

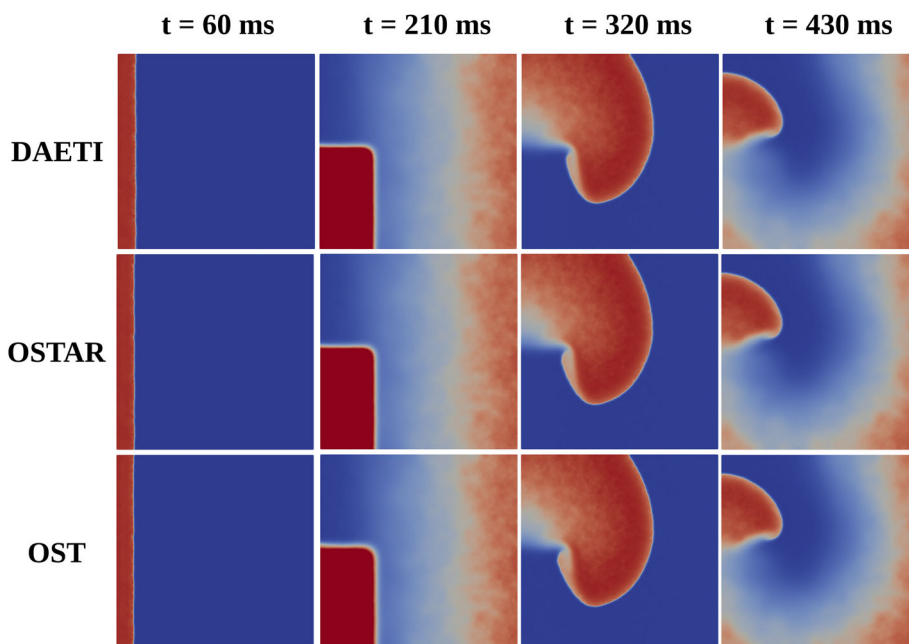


**FIGURE 2** Voltage snapshots in a 2D fibrotic tissue sheet in response to a cross-stimulation protocol. Spiral waves of the same characteristics can be observed for DAETI (top), OSTAR (middle) and OST (bottom) at different simulated time instants

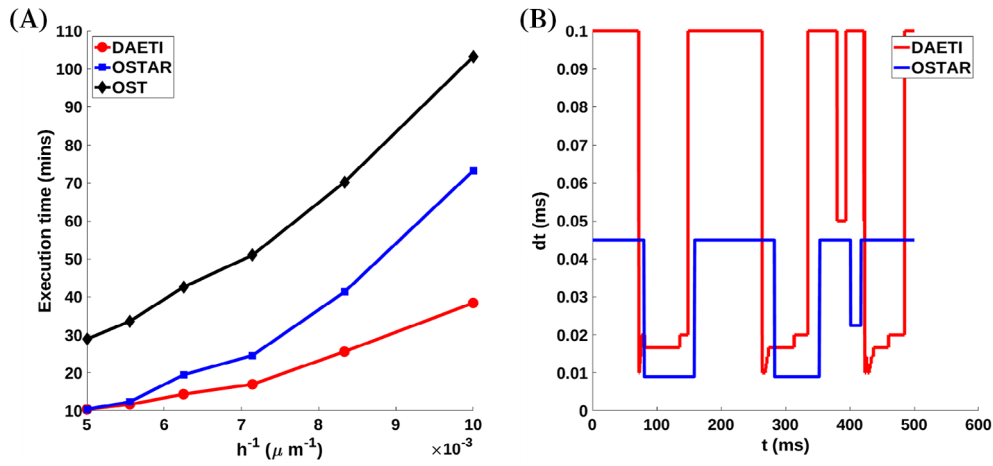


**FIGURE 3** (A) Execution time for DAETI (red circle), OSTAR (blue square) and OST (black diamond) evaluated in a 2D fibrotic tissue with 4-node regular element meshes and varying space steps ranging from  $h = 100$  to  $h = 200 \mu m$ , (B) temporal evolution of adaptive time step for DAETI (red) and OSTAR (blue)

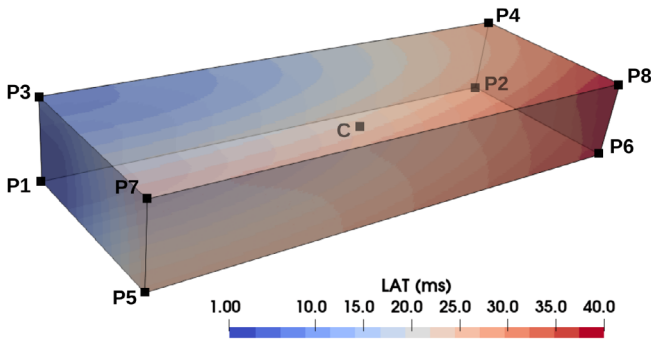


**FIGURE 4** Activation time map for the 3D cuboid benchmark geometry described in Reference 18 with space discretization  $h = 0.1$  mm

step  $dt$  over  $T = 500$  ms for the mesh with  $h = 200 \mu m$ . As can be observed from the figure,  $dt$  for OSTAR was bounded by the critical time step  $dt_s = 0.045$  ms, while DAETI was solved more efficiently using up to  $dt = 0.1$  ms.

### 3.3 | Electrical propagation in a 3D cuboid benchmark geometry

In this example, we considered the propagation of an electrical impulse in a homogeneous 3D cuboid of human ventricular tissue. We followed the simulation protocol described in Reference 18, in which a common benchmark problem for verification of cardiac tissue electrophysiology simulators was defined. The cuboid had dimensions  $3 \times 7 \times 20$  mm with cardiac fibers parallel to the Z axis. It was considered to be composed of human ventricular epicardial tissue, with the Ten Tusscher et al.<sup>19</sup> model used to describe cellular electrophysiology. The value of the diffusion coefficient in the longitudinal direction was set to  $d_0 = 0.00115$   $cm^2/ms$  and the transverse-to-longitudinal ratio was set to  $\rho = 0.12$ . A stimulus of 2 ms duration and 50 mA amplitude was delivered at a cube with dimensions  $1.5 \times 1.5 \times 1.5$  mm located at corner P1 (Figure 4).

In Reference 18, Niederer et al. reported activation times at the eight corners (P1 – P8) and at the center (C) of the cuboid for 11 different electrophysiology solvers. Results in that study were reported for three spatial discretizations,  $h = \{0.1, 0.2, 0.5\}$  mm, and three integration time steps,  $dt = \{0.005, 0.010, 0.050\}$  ms, while  $dt_s = \{0.230, 0.037, 0.009\}$  ms and  $dt_{CFL} = \{2.7, 0.5, 0.2\}$  ms. Here, we performed simulations for the three spatial discretizations using the DAETI method with  $dt = 0.1$  ms. In Table 2, the activation times obtained by DAETI are reported together with the average activation times produced by all the solvers tested in Reference 18 for comparison purposes. As it can be observed, activation times obtained with DAETI for the different spatial discretizations were in good agreement with the average activation times reported in Reference 18 and, in all cases, within the ranges reported for the different solvers.

**TABLE 2** Activation times at the corners (P1–P8) and at the center (C) of the 3D cuboid benchmark geometry defined in Reference 18

<b>h (mm)</b>	<b>P1</b>	<b>P2</b>	<b>P3</b>	<b>P4</b>	<b>P5</b>	<b>P6</b>	<b>P7</b>	<b>P8</b>	<b>C</b>
DAETI activation times (ms)									
0.5	1	49	22	58	94	109	98	111	54
0.2	1	31	11	35	35	51	39	54	25
0.1	1	29	8	31	27	41	29	43	20
Average activation times (ms) in Reference 18									
0.5	1	48	27	55	106	118	107	118	55
0.2	1	35	11	37	39	53	41	54	25
0.1	1	31	9	33	28	43	30	44	20

### 3.4 | Electrical propagation in a 3D cardiac biventricular geometry

We further compared the DAETI method with the OSTAR and OST methods in the simulation of AP propagation in a 3D biventricular swine geometry considering myocardial infarction and left bundle branch block (LBBB) conditions. A tetrahedral mesh representation of the biventricular swine anatomy (273919 nodes, 1334218 elements) was made available from the CRT-EPiggy19 challenge.<sup>20,21</sup> It was part of a swine model dataset of LBBB for experimental studies of cardiac resynchronization therapy.<sup>22,23</sup> A homogeneous diffusion coefficient  $d_0 = 0.002 \text{ cm}^2/\text{ms}$  was set across the cardiac tissue, with a transverse-to-longitudinal conductivity ratio of  $\rho = 0.25$ . For the myocardial infarction simulation, the scar region was located at the left anterior part of the left ventricle's apex and was assumed as zero conductive tissue. The scar border zone was not considered since it was not available in the anatomical model. The diffusion coefficient for the connective tissue at the base of the biventricular anatomy was set to  $d_0 = 0.00066 \text{ cm}^2/\text{ms}$ . The electrophysiology of connective tissue was represented by the MacCannell active fibroblast model. For the rest of the biventricular geometry, the O'Hara et al. cell model was used. Transmural heterogeneities were included by considering endocardial, midmyocardial and epicardial cells across the ventricular wall at 0.5:0.2:0.3 ratio. The orientation of the myocardial fibers was computed using a rule-based method.<sup>24</sup>

A Purkinje conduction system was generated for the biventricular model by using a fractal-tree generation algorithm.<sup>25</sup> Purkinje-myocyte junctions (PMJs) on the endocardial surface were obtained by applying a range-search algorithm using a spherical search area with radius  $R = 2 \text{ mm}$ , centered at each end node of the conduction system. Rather than considering AP propagation in the conduction system, periodic stimuli of 1 ms duration and twice diastolic threshold in amplitude were applied to each PMJ at a cycle length of 1000 ms. To ensure realistic activation at baseline conditions,<sup>26</sup> we divided PMJs into four groups: left apex - LA; left base - LB; right apex - RA; right base - RB. LA-PMJs were activated at time  $t = 0 \text{ ms}$ , while the activation of LB-PMJs, RA-PMJs, and RB-PMJs was delayed by 7, 4, and 11 ms, respectively. Under LBBB conditions, stimulation at LA-PMJs and LB-PMJs was blocked. After achieving steady-state, the total simulation time was  $T = 500 \text{ ms}$  for both myocardial infarction and LBBB simulations. The critical value for the diffusion time step was  $dt_s = 0.034 \text{ ms}$ , while  $dt_{CFL} = 0.16 \text{ ms}$ .

For both simulations, the results obtained by DAETI and OSTAR were compared against the results obtained by the OST simulation, taken here as a reference, by computing the normalized root mean square error for both the local activation time (LAT), denoted by  $e_{LAT}$ , and APD<sub>90</sub>, denoted by  $e_{APD}$ :

$$e_Z = \frac{\sqrt{\frac{1}{N} \sum_{i=1}^N (\hat{u}_i - u_i)^2}}{u_{max} - u_{min}}, \quad (4)$$

where the subindex Z stands for LAT or APD,  $N$  is the number of nodes in the mesh,  $u$  denotes the reference nodal value for either LAT or APD<sub>90</sub> obtained by OST and  $\hat{u}$  denotes the nodal LAT or APD<sub>90</sub> value obtained by OSTAR or DAETI.  $u_{max}$  and  $u_{min}$  denote the maximum and minimum values of  $u$  across all nodes in the tissue.

Using the DAETI method,  $e_{LAT}$  was 4.3E-3 and 4.4E-3 for infarction and LBBB simulations, respectively, whereas for the OSTAR method the corresponding  $e_{LAT}$  values were 3.0E-3 and 2.6E-3. In the case of  $e_{APD}$ , the values for DAETI were 1.6E-3 and 7.8E-4 for infarction and LBBB simulations, while for OSTAR these were 1.2E-4 and 7.1E-4.

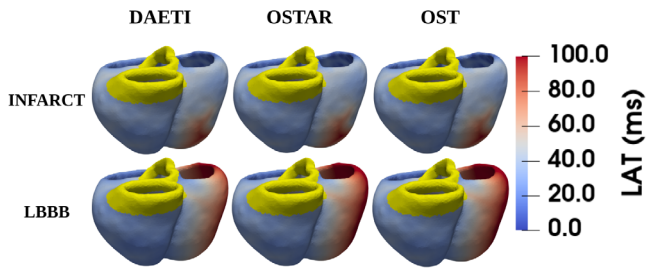


FIGURE 5 LAT maps at baseline (top) and under LBBB conditions (bottom) for a simulation using DAETI (left), OSTAR (middle) and OST (right) methods

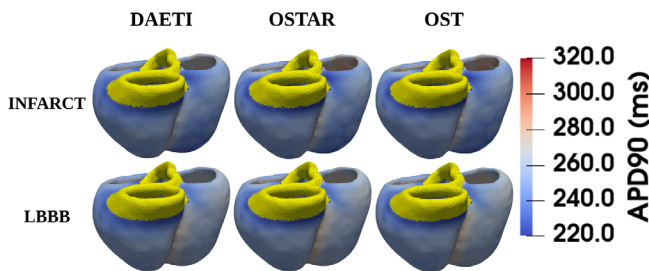


FIGURE 6 APD<sub>90</sub> maps at baseline (top) and under LBBB conditions (bottom) for a simulation using DAETI (left), OSTAR (middle) and OST (right) methods

Mean LAT was 27.2, 27.4, and 27.5 ms for DAETI, OSTAR, and OST in the infarction simulation. For LBBB simulation, mean LAT was 49.3, 49.7, and 49.9 ms, respectively. Mean APD<sub>90</sub> was 231.4 ms for infarction and 233.2 ms for LBBB with all three methods. Figures 5 and 6 show LAT and APD<sub>90</sub> maps for infarction and LBBB simulations. From Figure 5, it can be appreciated that epicardial activation under LBBB occurs by wave propagation through the interventricular septum and the anterior and posterior left ventricular wall. This characteristic activation pattern is well reproduced by the three numerical integration methods. Histograms of LAT and APD<sub>90</sub> for infarction and LBBB simulations are presented in Figure 7 as a measure of the distribution of LAT and APD<sub>90</sub> nodal values. DAETI results were in very good agreement with OST, as confirmed by the overlapping of the histograms.

In terms of computational efficiency, the total execution time at infarct conditions was 25.4 min for DAETI, 63.0 min for OSTAR, and 106.2 min for OST. Under LBBB conditions, the total execution time was 23.4 min for DAETI, 62.4 min for OSTAR, and 102.6 min for OST. Using the DAETI method we obtained a speed-up of 4.2× at infarct and 4.4× under LBBB with respect to OST. The speed-up obtained by OSTAR with respect to OST was 1.7× at infarct and 1.7× at LBBB conditions.

## 4 | DISCUSSION

We proposed a DAETI method to solve the monodomain model in cardiac electrophysiology. Our method is an extension of the operator splitting technique with adaptive reaction (OSTAR) where adaptive explicit integration is applied for the integration of the diffusion term too. Our approach is simple, yet efficient, and provides higher computational speed as compared to OSTAR. By introducing adaptive time stepping also for the explicit solution of the diffusion term, the conditional stability limitation can be overcome with small computational overhead, since the largest part of the required computational time is associated with the solution of the decoupled reaction term. The combination of adaptive time integration for both the diffusion and reaction terms in the DAETI method allows achieving a computational speed-up of up to 2.7× in 2D tissue simulations and 4.4× in 3D biventricular simulations when compared to simulations performed with OST without time adaptivity. Using adaptive integration only for the reaction term in the OSTAR method, the computational speed-up is limited to 1.4× and 1.8× for the same 2D and 3D simulations. Based on these findings, we can conclude that the DAETI method is notably more computationally efficient than OSTAR, especially for 3D realistic models.

The DAETI method demonstrated good numerical accuracy compared to OST without time adaptivity. In 2D tissue simulations, differences in LAT and APD<sub>90</sub> calculated at the center of the tissue were found only for the atrial tissue simulation. Percentage difference for CV was up to 5.6% (0.056 cm/ms in DAETI, 0.053 cm/ms in OST) and for APD<sub>90</sub> was up to 0.5% (208 ms in DAETI, 209 ms in OST). These results were as expected, since small voltage differences in



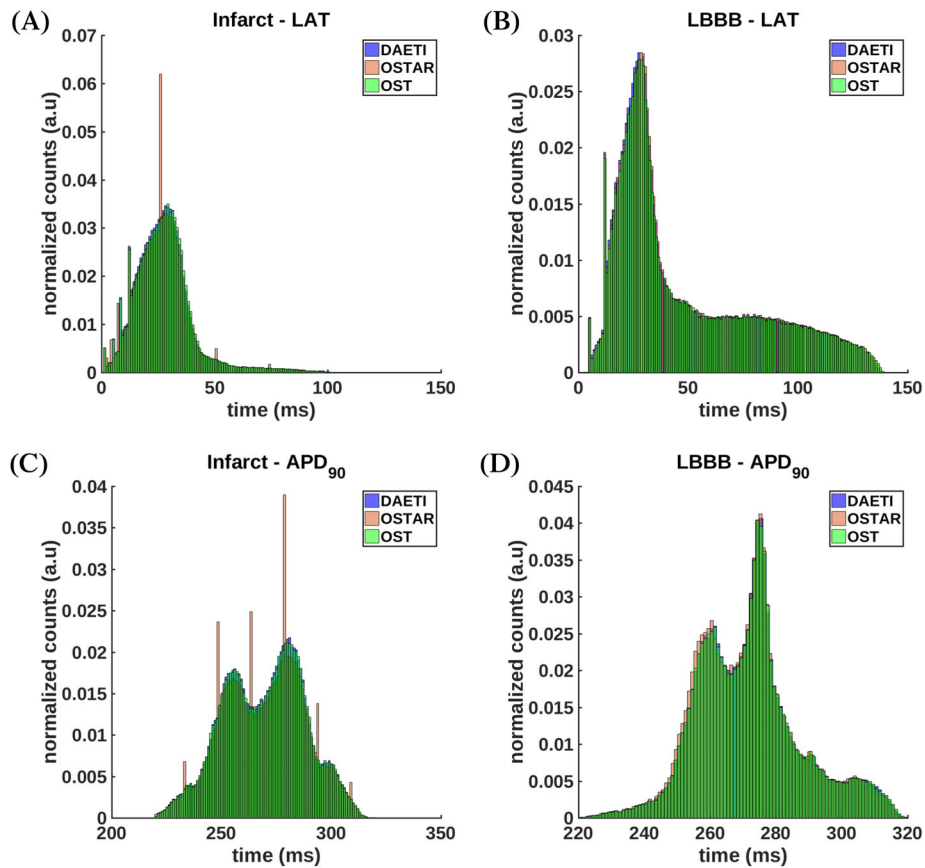


**FIGURE 7** Histogram showing the distributions of nodal values using DAETI (blue), OSTAR (orange) and OST (green) for (A) LAT under myocardial infarction conditions, (B) LAT under LBBB conditions, (C)  $APD_{90}$  under myocardial infarction conditions and (D)  $APD_{90}$  under LBBB conditions

the AP upstroke due to numerical approximation contribute mainly to CV and not to  $APD_{90}$ , which is calculated from the time point associated with maximum AP derivative and it is largely controlled by the recovery process.<sup>4</sup> The OSTAR method led to increased CV by 3.8% as compared to OST. From these findings we can conclude that the CV increase in DAETI due to the adaptive integration of the diffusion term is 1.8%. In Reference 4, the increase in CV due to time adaption for the reaction term is less than 2% even for a time integration step as large as  $dt = 0.4$  ms. In our study, the increase in CV is larger even if the time integration step  $dt = 0.1$  ms is smaller. It should, however, be noted that simulations in Reference 4 are performed in 1D cables, while ours correspond to 2D and 3D tissues, which suggests that the increase in CV associated with adaptive integration of the reaction term may be larger for higher dimensions.

In the simulation of the 3D cuboid benchmark we observed that DAETI led to activation time measurements in very good agreement with state-of-the-art electrophysiology solvers.<sup>18</sup> Using biventricular geometries, very good agreement was found between DAETI and either OSTAR or OST in terms of both LAT and  $APD_{90}$ . Taking OST as a reference, both DAETI and OSTAR rendered error values of  $e_{LAT}$  and  $e_{APD}$  of the order of E-3 and E-4, respectively, at infarct and LBBB conditions. The activation pattern characteristic of LBBB conditions, as well as the longer time required to fully complete ventricular activation under these conditions, were well represented by DAETI, OSTAR and OST, providing results in agreement with previously published data.<sup>23,27</sup>

The findings of this study confirmed that the proposed DAETI method can be effectively used to simulate cardiac electrophysiology under physiological and pathophysiological conditions, with similar numerical accuracy and remarkably higher efficiency than OSTAR, especially for 3D simulations. Importantly, by applying adaptive integration to the explicit solution of the diffusion term, the conditional stability limitation of the explicit schemes was overcome. For all the above characteristics, the DAETI method is suggested as an attractive technique for the solution of large scale problems. Since explicit schemes are highly parallelizable, we expect to observe a significantly higher efficiency gain in a parallel computing architecture implementation.

In future work, we plan to implement an MPI parallel version of the DAETI method and compare its scalability against semi-implicit methods in large scale 3D applications. Furthermore, we aim to use DAETI to explore in depth the role of fibrosis in the generation of arrhythmia. While in this study we considered only diffuse fibrosis, which is common in patients with congenital heart disease<sup>28</sup> or heart failure,<sup>29</sup> in future works we plan to investigate the relationship between both diffuse and patchy fibrosis with arrhythmia generation, with a particular interest in modeling cardiac activity following myocardial infarction.

## 5 | CONCLUSION

A DAETI method is proposed to solve the monodomain model in 2D and 3D cardiac electrophysiology simulations. DAETI is based on the simple yet efficient realization that adaptive time integration can be used for the explicit solution of the diffusion term, on top of the reaction term, in the monodomain model after decoupling these two terms by the operator splitting technique. In a set of 2D and 3D simulations of cardiac electrical propagation in health and disease, the DAETI method is shown to render results of similar accuracy but improved computational efficiency than operator splitting-based methods with and without adaptive integration of the reaction term. As a fully explicit technique, the application of DAETI is expected to provide even higher efficiency gain in parallel implementations due to its straightforward parallelization and high scalability.

## ACKNOWLEDGMENTS

This work was supported by the European Research Council under grant agreement ERC-StG-638284, by Ministerio de Ciencia e Innovación (Spain) through project PID2019-105674RB-I00 and by European Social Fund (EU) and Aragón Government through BSICoS group (T39\_20R) and project LMP124-18. Computations were performed by the ICTS NANBIOSIS (HPC Unit at University of Zaragoza).

## DATA AVAILABILITY STATEMENT

The data that support the findings of this study are available from the corresponding author upon reasonable request.

## ORCID

Konstantinos A. Mountris  <https://orcid.org/0000-0003-2946-3044>

Esther Pueyo  <https://orcid.org/0000-0002-1960-407X>

## REFERENCES

1. Tung L. *A Bi-domain Model for Describing Ischemic Myocardial DC Potentials* [PhD thesis]. Massachusetts Institute of Technology; 1978.
2. Keener JP, Sneyd J. *Mathematical Physiology: Systems Physiology. II*. New York: Springer; 2009.
3. Potse M, Dubé B, Richer J, Vinet A, Gulrajani RM. A comparison of monodomain and bidomain reaction-diffusion models for action potential propagation in the human heart. *IEEE Trans Biomed Eng*. 2006;53(12):2425-2435.
4. Qu Z, Garfinkel A. An advanced algorithm for solving partial differential equation in cardiac conduction. *IEEE Trans Biomed Eng*. 1999; 46(9):1166-1168.
5. Gomes JM, Oliveira RS, Lobosco M, dos Santos RW. Adaptive-step methods for markov-based membrane models. *Commun Nonlinear Sci Numer Simul*. 2020;85:105249.
6. Heidenreich EA, Ferrero JM, Doblaré M, Rodríguez JF. Adaptive macro finite elements for the numerical solution of monodomain equations in cardiac electrophysiology. *Ann Biomed Eng*. 2010;38(7):2331-2345.
7. Rush S, Larsen H. A practical algorithm for solving dynamic membrane equations. *IEEE Trans Biomed Eng*. 1978;4:389-392.
8. Courant R, Friedrichs K, Lewy H. On the partial difference equations of mathematical physics. *IBM J Res Dev*. 1967;11(2):215-234.
9. Myers GE. The critical time step for finite-element solutions to two-dimensional heat-conduction transients. *J Heat Transfer*. 1978;100(1):120-127.
10. Lloyd CM, Lawson JR, Hunter PJ, Nielsen PF. The CellML model repository. *Bioinformatics*. 2008;24(18):2122-2123.
11. Mountris KA, Sanchez C, Pueyo E. A novel paradigm for in silico simulation of cardiac electrophysiology through the mixed collocation meshless Petrov-Galerkin method. Paper presented at: 2019 Computing in Cardiology (CinC); September 8-11, 2019; Singapore:IEEE.
12. Mountris KA, Pueyo E. Next-generation in silico cardiac electrophysiology through immersed grid meshfree modeling: application to simulation of myocardial infarction. Paper presented at: 2020 Computing in Cardiology (CinC); September 13-16, 2020; Rimini, Italy: IEEE.
13. Mountris KA, Pueyo E. The radial point interpolation mixed collocation method for the solution of transient diffusion problems. *Eng Anal Bound Elem*. 2020;121:207-216.

14. Maleckar MM, Greenstein JL, Trayanova NA, Giles WR. Mathematical simulations of ligand-gated and cell-type specific effects on the action potential of human atrium. *Prog Biophys Mol Biol*. 2008;98(2-3):161-170.
15. O'Hara T, Virág L, Varró A, Rudy Y. Simulation of the undiseased human cardiac ventricular action potential: model formulation and experimental validation. *PLoS Comput Biol*. 2011;7(5):e100206.
16. Gomez JF, Cardona K, Martinez L, Saiz J, Trenor B. Electrophysiological and structural remodeling in heart failure modulate arrhythmogenesis. 2D simulation study. *PLoS One*. 2014;9(7):e103273.
17. MacCannell KA, Bazzazi H, Chilton L, Shibukawa Y, Clark RB, Giles WR. A mathematical model of electrotonic interactions between ventricular myocytes and fibroblasts. *Biophys J*. 2007;92(11):4121-4132.
18. Niederer SA, Kerfoot E, Benson AP, et al. Verification of cardiac tissue electrophysiology simulators using an N-version benchmark. *Philos Trans R Soc A: Math Phys Eng Sci*. 2011;369(1954):4331-4351.
19. Ten Tusscher KH, Panfilov AV. Alternans and spiral breakup in a human ventricular tissue model. *Am J Physiol Heart Circ Physiol*. 2006;291(3):H1088-H1100.
20. Camara O. Best (and worst) practices for organizing a challenge on cardiac biophysical models during AI summer: the CRT-EPiggy19 challenge. Paper presented at: International Workshop on Statistical Atlases and Computational Models of the Heart: 2019; Springer: 329-341.
21. Pop M, Sermesant M, Camara OCR, et al. Statistical atlases and computational models of the heart: multi-sequence CMR segmentation, CRT-EPiggy and LV full quantification challenges. Paper presented at: 10th International Workshop, STACOM 2019, Held in Conjunction with MICCAI 2019; October 13, 2019; Shenzhen, China, Revised Selected Papers, vol. 12009. Springer Nature; 2020.
22. Rigol M, Solanes N, Fernandez-Armenta J, et al. Development of a swine model of left bundle branch block for experimental studies of cardiac resynchronization therapy. *J Cardiovasc Transl Res*. 2013;6(4):616-622.
23. Iglesias DS, Duchateau N, Butakov CBK, et al. Quantitative analysis of electro-anatomical maps: application to an experimental model of left bundle branch block/cardiac resynchronization therapy. *IEEE J Transl Eng Health Med*. 2016;5:1-15.
24. Doste R, Soto-Iglesias D, Bernardino G, et al. A rule-based method to model myocardial fiber orientation in cardiac biventricular geometries with outflow tracts. *Int J Numer Methods Biomed Eng*. 2019;35(4):e3185.
25. Costabal FS, Hurtado DE, Kuhl E. Generating Purkinje networks in the human heart. *J Biomech*. 2016;49(12):2455-2465.
26. Durrer D, Van Dam RT, Freud G, Janse M, Meijler F, Arzbaecher R. Total excitation of the isolated human heart. *Circulation*. 1970;41(6):899-912.
27. Van Dam RT. Ventricular activation in human and canine bundle branch block. *The Conduction System of the Heart*. Dordrecht: Springer; 1978:377-392.
28. Broberg CS, Chugh SS, Conklin C, Sahn DJ, Jerosch-Herold M. Quantification of diffuse myocardial fibrosis and its association with myocardial dysfunction in congenital heart disease. *Circ Cardiovasc Imaging*. 2010;3(6):727-734.
29. Iles L, Pfluger H, Phrommintikul A, et al. Evaluation of diffuse myocardial fibrosis in heart failure with cardiac magnetic resonance contrast-enhanced T1 mapping. *J Am Coll Cardiol*. 2008;52(19):1574-1580.

**How to cite this article:** Mountris KA, Pueyo E. A dual adaptive explicit time integration algorithm for efficiently solving the cardiac monodomain equation. *Int J Numer Meth Biomed Engng*. 2021;e3461. <https://doi.org/10.1002/cnm.3461>